


Hyperosmolality in CHO culture: Effects on cellular behavior and morphology

Nadiya Romanova¹ | Tarek Niemann^{2,3} | Johannes F. W. Greiner³  |
Barbara Kaltschmidt^{2,3} | Christian Kaltschmidt³ | Thomas Noll¹ 

¹Cell Culture Technology, Faculty of Technology, Bielefeld University, Bielefeld, Germany

²AG Molecular Neurobiology, Faculty of Biology, Bielefeld University, Bielefeld, Germany

³Department of Cell Biology, Faculty of Biology, University of Bielefeld, Universitaetsstrasse 25, Bielefeld, 33615, Germany

Correspondence

Thomas Noll, Bielefeld University, Universitaetsstr. 25, 33615 Bielefeld, Germany.
Email: Thomas.Noll@uni-bielefeld.de

Abstract

Exposure of Chinese hamster ovary cells (CHO) to highly concentrated feed solution during fed-batch cultivation is known to result in an unphysiological osmolality increase (>300 mOsm/kg), affecting cell physiology and morphology. Extending previous observation on osmotic adaptation, the present study investigates for the first time potential effects of hyperosmolality on CHO cells on both population and single-cell level. We intentionally exposed CHO cells to hyperosmolality of up to 545 mOsm/kg during fed-batch cultivation. In concordance with existing research data, hyperosmolality-exposed CHO cells showed a nearly triplicated volume accompanied by ablation of proliferation. On the molecular level, we observed a strong hyperosmolality-dependent increase in mitochondrial activity in CHO cells compared to control. In contrast to mitochondrial activity, hyperosmolality-dependent proliferation arrest of CHO cells was not accompanied by DNA accumulation or caspase-3/7-mediated apoptosis. Notably, we demonstrate for the first time a formation of up to eight multiple, small nuclei in single hyperosmolality-stressed CHO cells. The here presented observations reveal previously unknown hyperosmolality-dependent morphological changes in CHO cells and support existing data on the osmotic response in mammalian cells.

KEYWORDS

cell morphology, cell size, CHO, fed-batch, hyperosmolality, mitochondria

1 | INTRODUCTION

Up to date, the majority of biopharmaceuticals, such as antibodies or their fragments, growth factors, cytokines, and Fc-fusion proteins are produced in mammalian cell lines. The ability of these cells to promote proper protein folding, replicate human-like posttranslational modifications, coupled with their high cell-specific productivity and ability to grow in suspension makes these cell lines highly (Fischer et al., 2015; Kim et al., 2011). Chinese hamster ovary (CHO)

cell-based protein production systems are by far the most commonly used in industry, accounting for 84% of the monoclonal antibody (mAb) products approved up to 2018 (Walsh, 2018).

CHO production processes are usually performed in a fed-batch mode using repeated bolus or continuous feeding, which leads to increased cell density and product titers. The high nutrient content of the medium concentrates being used can result in a substantial increase in medium osmolality, which is known to affect cellular behavior and productivity (Bibila & Robinson, 1995; Ryu & Lee, 1999).

N. Romanova and T. Niemann contributed to the manuscript equally.

This is an open access article under the terms of the Creative Commons Attribution-NonCommercial-NoDerivs License, which permits use and distribution in any medium, provided the original work is properly cited, the use is non-commercial and no modifications or adaptations are made.

© 2021 The Authors. *Genetic Epidemiology* Published by Wiley Periodicals LLC

Several studies have investigated the effects of osmolality change on the growth and productivity of CHO cells (Kiehl et al., 2011; Pan et al., 2017; Shen et al., 2010). In most cases an increased cell-specific productivity (Nasseri et al., 2014; Qin et al., 2019; Takagi et al., 2000; Wang et al., 2012) with concomitant depressed cell growth (Kim & Lee, 2002) has been found, but also an increase in cell size under hyperosmolality has been reported. This seems to be inconsistent with classical osmosis that should result in cells' shrinking by loss of cytoplasmic water, as observed in bacteria (Dai & Zhu, 2018) and yeast (Pratt et al., 2003). Exposed to high osmolality, mammalian cells decrease in volume for about first 30 min (Kiehl et al., 2011). This cell shrinkage induces a reactive oxygen species (ROS) formation, catalyzed by a NADPH oxidase (Schliess et al., 2007).

To further investigate the underlying mechanisms of the cell size increase and to obtain a more holistic overview of the effect of hyperosmolality on CHO cells, we intentionally "overfed" the antibody-producing CHO DP-12 cells with specifically tailored industrially relevant CHO feed and studied the effects of osmolality increase on a populational and single-cell level.

2 | MATERIALS AND METHODS

2.1 | Cell culture maintenance

The influence of high osmolality was studied primarily in suspension-adapted CHO DP-12 clone#1934 (ATCC CRL-12445) cells. It co-expressed the variable light and heavy chains of the murine 6G4.2.5 monoclonal antibody (ATCC-HB-11722) which inhibits binding of interleukin-8 (IL-8) to human neutrophil. Gene integration was stabilized by DHFR/MTX system. The 200 nM methotrexate (MTX, Sigma-Aldrich) was present during preculture but not during the main cultivation. CHO DP-12 cells were cultivated in chemically defined medium TCX6D (Xell AG) supplemented with 8 mM glutamine.

For each experimental cultivation a new vial containing 1×10^7 cells was thawed, washed in phosphate-buffered saline (PBS) once, and resuspended in ca. 15 ml of growth medium. All vials originated from the same master cell bank. Pre-culture was maintained in vented conical flasks (50 ml TubeSpin, TPP Techno Plastic Products AG) and routinely passaged every 3 days. Cell concentration, viability, and cell diameter were determined with a Cedex AS20 system (Innovatis-Roche AG). Each measurement was based on 20 valid images. The parameters of about 200 to up to 8000 cells were measured per sample. Cells were seeded with a viable cell density (VCD) of 3×10^5 cells/ml.

Incubation parameters in an orbital shaker incubator (Mytron GmbH) were maintained at 37°C with a relative CO₂ concentration of 5%, 80% humidity, and with shaker agitation of 185 rpm.

2.2 | Fed-batch cultivation

Cells for three to four biological replicates for each of two conditions ("feed" condition and "control" condition) were seeded with a VCD of

3×10^5 cells/ml in a 125 ml polycarbonate un-baffled shake flask (Corning Life Sciences B.V.) in an initial volume of 40 ml and cultivated as described before.

For feed-condition shakers, CHO Basic Feed (Xell AG) was supplemented with 404 mM glucose, 70 mM glutamine, and 27 mM asparagine. About 72 h post-seeding, 6 ml of supplemented feed were added to the feed-condition shakers for the first time. This procedure was repeated four times in total, roughly once every 24 h. To cancel out any dilution effects, 6 ml of the Gln-supplemented growth medium was added to control-condition shakers at the same time points.

The product (anti-IL-8 antibody) concentration was estimated using Protein A HPLC after finishing the cultivation. Daily glucose and lactate measurements were performed using cell-free supernatant on a Biosen C-line Clinic (GEMAR GmbH). Osmolality was measured daily using an Osmomat Auto (Gonotec GmbH).

2.3 | Cell cycle analysis

Cell cycle distribution was analyzed on BioRad S3E (BioRad Laboratories Inc.) Data were evaluated with FlowJo™ v10.6.2 (FlowJo, now BD Bioscience) software. About 2×10^6 cells were harvested at four designated time points (Day 2, 4, 5, and 7), washed twice with ice-cold PBS, permeabilized with ice-cold 70% ethanol, and stored at -20°C at least overnight. Before measurement, cells were washed twice with 0.1% saponin in PBS, followed by incubation for 45 min in the dark at room temperature with 20 µg/ml/ 10^6 cells propidium iodide (PI) and 40 µg/ml/ 10^6 cells RNase A. After the incubation, cells were stored on ice and vortexed before each measurement and strained through nylon-mesh CellTrics filters with 30 µm pore size (Sysmex, Kōbe) directly into the measuring tube. About 180,000 events per sample were collected at a low acquisition rate (200–300 cells/s). The PI fluorescence is proportional to the DNA content of the cell and was detected in the FL2 channel.

2.4 | Mitochondria activity assessment

MitoTracker® Red CMXRos (Cell Signalling Technology Inc.) reagent was used to characterize mitochondrial mass and activity in the cells using flow cytometry. The dye is sensitive to mitochondrial membrane potential and can be used to access the functionality of mitochondria (Puleston, 2015). It diffuses passively through the cell membrane and accumulates in active mitochondria. CMXRos is a nontoxic sensitive indicator of relative changes in membrane potential $\Delta\Psi_m$ (Pendergrass et al., 2004). It also has the advantage to be retained in the organelles after methanol fixation (Macho et al., 1996). 1.5×10^6 cells were sampled from each shaker at three designated time points (Day 2, 6, and 8), centrifuged at $200 \times g$ and resuspended in 100 nM MitoTracker® Red CMXRos reagent diluted in growth medium to a concentration of 2×10^6 cells/ml. The samples were incubated at 37°C on an orbital shaker (185 rpm) for 45 min in

the dark. Nuclei were counterstained with 1 μ M 4',6-diamidino-2-phenylindol (DAPI, 1:1000 dilution of 1 mM DAPI stock, Sigma, now Merck) for 10 min at 37°C. Following the counterstaining step, cells were strained through nylon-mesh CellTrics filters with 30 μ m pore size (Sysmex, Kōbe) directly into flow cytometry tube.

Measurement was performed on Navios EX flow cytometer (Beckman Coulter). Dead cells were gated out based on DAPI signal and intensities of MitoTracker stained cell populations were compared at an emission maximum of 561 nm.

2.5 | Apoptosis assay

An apoptotic signal was detected by assaying intracellular Caspase 3/7 activation using CellEvent® Caspase-3/7 Green Detection Reagent (Thermo Fisher Scientific Inc.), which is not toxic to the cells. It is an Asp-Glu-Val-Asp (DEVD) peptide, conjugated to a nucleic acid binding dye. This conjugate is cell-permeable but intrinsically non-fluorescent unless it is bound to the DNA. The DEVD peptide inhibits the ability of the dye to bind DNA and must be cleaved away by an activated Caspase 3 or Caspase 7 protease for fluorescence to occur. The bright green signal was detected at 514 nm on Navios EX flow cytometer.

About 1.5×10^6 cells were collected at the previously indicated time points, centrifuged at $200 \times g$ for 5 min. and resuspended in 300 μ l of growth medium with the same osmolality. The Caspase 3/7 reagent was added in a concentration of 5 μ M to the positive samples, the same volume of the growth medium was added as vehicle control. Both positive and negative samples were incubated for 30 min at 37°C, 5% CO₂ and humidity of 80% without shaking. The cells were not washed throughout the whole preparation process to preserve a native cell distribution. After the incubation cells were counterstained with DAPI at 1 μ M and incubated for 10 min as before. Before measurement, the cells were diluted to a final concentration of 2×10^6 cells/ml and strained through nylon-mesh CellTrics filters with 30 μ m pore size (Sysmex, Kōbe) directly into flow cytometry tube. The flow cytometry analysis was conducted immediately after the incubation.

2.6 | Confocal microscopy and immunocytochemistry (ICC)

Samples for all confocal microscopy analyses were taken at the same time points as those for proteome and live-stains: at Days 2, 6, and 8. Only one biological replicate per feed and control conditions was examined. The mitochondria live stain MitoTracker® Red CMXRos and Caspase 3/7 green detection reagent can be used for an end-point assay if a sample is fixed immediately after incubation.

For confocal microscopy, 0.5×10^6 cells were sampled from one of the shakers per condition. The sample was stained with 200 nM MitoTracker® Red CMXRos for 45 min at 37°C on an orbital shaker (185 rpm) in the dark. To omit a bright red background, the sample

was washed three times with PBS and then fixed in 250 μ l of 100% ice-cold methanol for 15 min at -20°C according to manufacturer instructions.

Samples stained for apoptosis detection via Caspase 3/7 activation (incubated for 30 min at 37°C, 5 μ M Caspase 3/7 green detection reagent) were fixed with 4% polymeric formaldehyde (PFA, Carl Roth GmbH) for 20 min at room temperature. The 100 μ l of each readily fixed sample were spun down onto ibidi 8 - chamber slides with ibidi-treat surface (ibidi GmbH) at $800 \times g$.

Samples with stained mitochondria were permeabilized and blocked in TritonX-100 (AppliChem) with 5% goat serum for 30 min. Ribosomal protein S6 (54D2) was stained with primary conjugated mouse mAb (S6 ribosomal protein [54D2, Alexa Fluor® 488 conjugate], #5317, Cell Signalling Technology Inc.) in 1:10,000 dilution.

The actin cytoskeleton was visualized by incubating 1:10 phalloidin rhodamine stock dilution (Sigma-Aldrich) for 10 min at room temperature (RT).

As of last, nuclear counterstaining was performed for all samples with DAPI (1:1000 dilution of 1 mM stock, Sigma-Aldrich) for 15 min at RT. DAPI is widely used for DNA visualization. It binds strongly to adenosine-thymidine (A-T) rich regions of nuclear DNA via electrostatic interactions (Hayashi et al., 1992; Tarnowski et al., 1991). DAPI staining followed by mounting with Mowiol 4-88 on 8 chamber ibidi slides. The mountant was allowed to cure for at least 48 h. Confocal laser scanning microscopy (LSM 780, Carl Zeiss) with ZEN software Version 2.3 was used for image acquisition. The data was processed by GraphPad Prism Software (GraphPad Software; Table 1).

3 | RESULTS AND DISCUSSION

3.1 | Cellular growth and cell size analysis

3.1.1 | CHO DP-12 cells exposed to osmolality elevation show proliferation depression and cell size increase

After an initial adaptation phase, the CHO DP-12 cells start to grow exponentially (Figure 1a). About 72 h post-seeding, 6 ml of supplemented feed was added (pure feed: 830 mOsm/kg) to the “feed” condition (in the following, referred to as “F”) or growth medium (306 mOsm/kg) to the control condition (in the following referred to as “C”). The osmolality in the control condition remained unchanged throughout the cultivation, except for a typical decrease to about 250 mOsm/kg on Day 8 due to the depletion of substrates in the medium. The addition of the supplemented feed caused a step-wise increase of osmolality in F from the initial physiological level of 304 ± 2 mOsm/kg to 545 ± 3 mOsm/kg in four increments (Figure 1b). The first two feedings bringing the mean osmolality up to 460 ± 3 mOsm/kg were sufficient to induce complete proliferation arrest accompanied by the onset of cell size increase measured by Cedex AS 20. The distribution of the cell size populations on Days 2, 4, 6, and 8 are shown in Figure 1c. The cells in the feed condition

TABLE 1 Selection of staining reagents and their targets in CHO cells used to characterize cell size increase on single-cell plane

Target	Staining reagent	Used concentration	Excitation wavelength
Mitochondria	MitoTracker® Red CMXRos ^a	200 nM	561 nm
Apoptosis activation	CellEvent® Caspase-3/7 Green Detection Reagent ^b	5 μM	488/514 nm
Ribosomes	S6 Ribosomal Protein (54D2) Mouse mAb Alexa Fluor® 488 Conjugate antibody ^a	1:400 dilution	488 nm

Abbreviation: CHO, Chinese hamster ovary.

^aCell Signalling Technology, Cambridge, UK.

^bThermo Fisher Scientific, Waltham, MA.

reached an average diameter of $20.8 \pm 0.3 \mu\text{m}$ (the mean between Days 7, and 10), which corresponds to the cell volume of $3784.9 \pm 0.3 \text{ fL}$ assuming a perfectly spherical form. Compared with the cells in control conditions (mean diameter days 7–10: $14.7 \pm 0.9 \mu\text{m}$, volume $1329.2 \pm 1.2 \text{ fL}$) this corresponds to a 39% increase in cell diameter and $\times 2.7$ increase in cell volume. The data shown here were observed for at least three independent experiments following the same set-up. We found out that the cell size increase is a reversible phenomenon: CHO cells previously exposed to high osmolality feed return to their normal size of $15 \pm 2.0 \mu\text{m}$ and start proliferating normally upon return into physiological conditions within roughly 48 h (data not shown).

While mammalian cells significantly vary in size between the cell types, the cell size is narrowly constrained for the given cell type and cultivation condition (Cadart et al., 2018). During the logarithmic phase in a normal fed-batch, the cell size is narrowly distributed between 12.5 and 18.0 μm (Figure 1c, blue bars), obviously showing a consistent pattern between cell cycle duration, biomass accumulation, and cell doublings. These processes are synergistically regulated and depend on each other (Cadart et al., 2018). On Day 8, almost 80% of the cells in the control are confined between 12.5 and 18.0 μm (Figure 1c). Cells in the “feed” on the contrary, show a broader cell-size distribution pattern where the main population shifts progressively to the 18.0–25.0 μm gate resulting in the shift of the average diameter. A similar broadening of cell-size distribution patterns for CHO cells exposed to osmolality increase has been reported previously (Kiehl et al., 2011; Pan et al., 2017). However, even if the osmolality gradient was set much steeper, achieving about $630 \pm 7 \text{ mOsm/kg}$ after four feedings, the average CHO DP-12 cell diameter did not exceed the maximum of $22.3 \pm 0.3 \mu\text{m}$ (unpublished data).

3.1.2 | Cell cycle distribution analysis shows no increase in DNA content in “feed” cells

Furthermore, we studied the distribution of DNA content in non-proliferating (hyperosmolality exposed) and normally growing CHO cells. The cells under control condition show a smooth transition from haploid (1N) G_0/G_1 to diploid (2N) G_2/M phase with clearly distinguishable S-phase (Figure 1e). The cells in the feed seem to be

arrested either in G_0/G_1 or in the G_2/M phase but lack the transition S-phase. The accumulation of 1N and 2N cells combined with concomitant depletion of the S-phase has been shown for yeast (Alexander et al., 2001) and recently for the CHO cells (Pan et al., 2019), exposed to osmotic pressure. There seems to be no trend of accumulating more than 2N DNA cells specific to one of the conditions. Thus, we conclude that the cells in “feed” increase in diameter, but do not generate more DNA (Li et al., 2017).

Exposure of CHO DP-12 cells to high-osmolality feed causes proliferation arrest coinciding with gradually progressing cell size increase. The cells in “feed” reside either in G_0/G_1 or in the G_2/M phase but lack the transition S-phase. Several existing studies in CHO (Bi et al., 2004), human cells (Demidenko & Blagosklonny, 2008), and budding yeast (Neurohr et al., 2019) show that the cells continue to increase in size if cell cycle progression is blocked by either external or internal factors. Our data suggests that cell exposure to osmolality well above the physiological level promotes cell cycle and DNA replication arrest. This, in turn, causes an increase in cell size due to continued biomass production.

3.2 | Assessment of mitochondrial activity and apoptosis induction via flow cytometry

3.2.1 | High osmolality feed causes an increase in mitochondrial membrane potential

Mitochondria are the main oxygen consumer of the cell, using 85% of the total amount assimilated by the cell for electron transport (Ademowo et al., 2017; Chan, 2006).

Mitochondria-specific marker MitoTracker chloromethyl-X-rosamine (CMXRos) used in this study is a thiol-reactive lipophilic dye, able to passively diffuse across the plasma membrane and to accumulate in active mitochondria (Poot et al., 1996). Its ability to do so depends on mitochondrial membrane potential $\Delta\Psi_m$: A more negative or polarized $\Delta\Psi_m$ will accumulate more dye, and vice versa. The membrane potential is in turn an important mitochondrial physiological parameter and relates to the cells' ability to produce ATP, which is decisive for oxygen consumption in mitochondria. Thus, the fluorescence intensity of the MitoTracker CMXRos dye shows a combined effect of (1) mitochondrial membrane potential $\Delta\Psi_m$

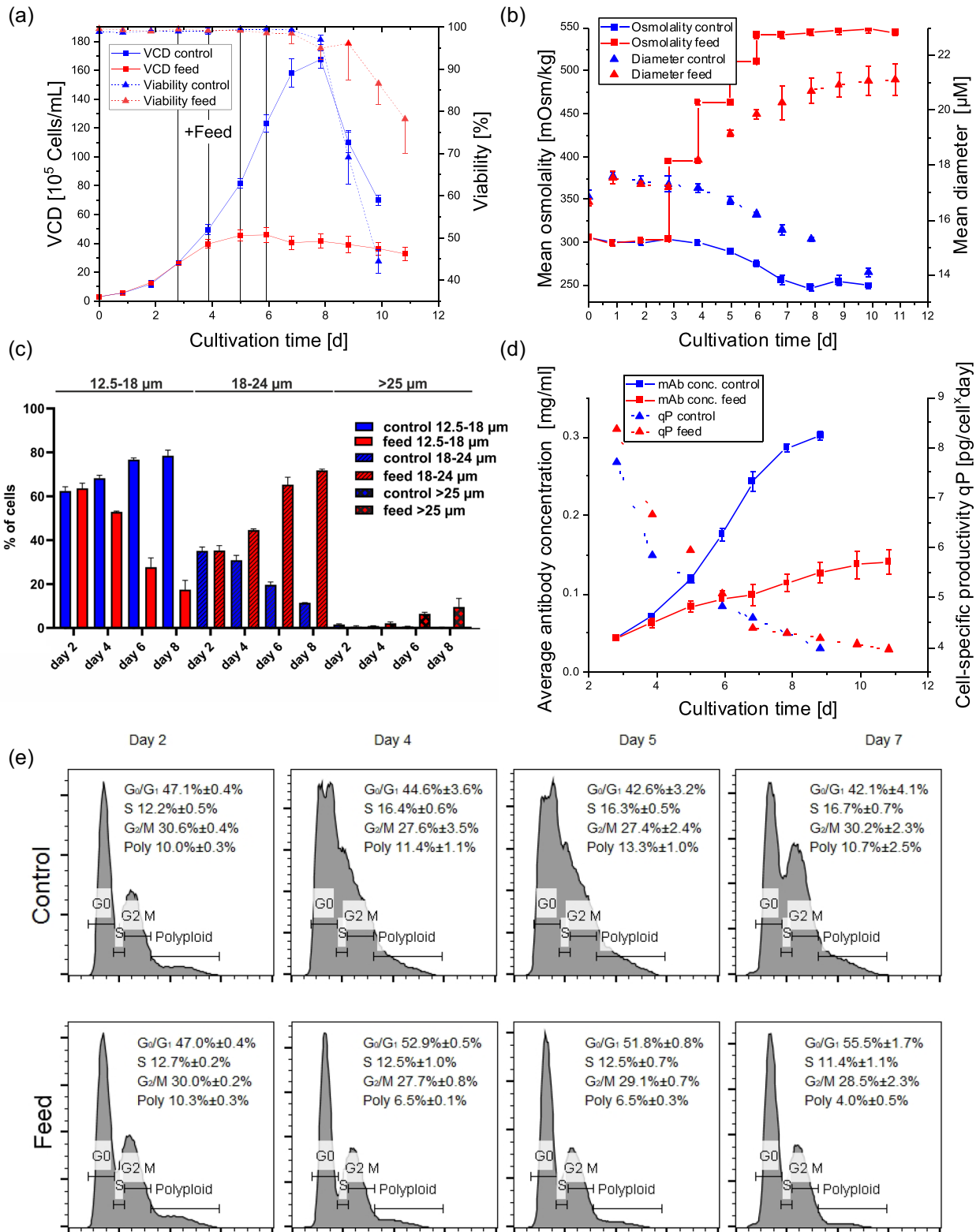


FIGURE 1 (See caption on next page)

which indicates health and activity of mitochondria in the cell (Cottet-Rousselle et al., 2011), and (2) is entangled with the amount of the mitochondrial membrane (Gilson et al., 2003), which depends on size and number of the mitochondria in the cell.

As an elevation of cell-specific oxygen uptake in CHO cells exposed to osmotic stress has been reported previously (Pan et al., 2017), we hypothesized that mitochondrial functionality plays a prominent role in cells' adaptation and survival in our set-up. Thus, we anticipated finding a difference in mitochondrial fluorescence based on the MitoTracker-labeling between the "feed" and "control" conditions.

In agreement with our hypothesis, we detected a significant ($p \leq 0.05$) fluorescence increase of MitoTracker-labeled mitochondria using flow-cytometry on Days 6 and 8 in the "feed" compared with the same time points in the "control" condition (Figure 2a). We used an unpaired parametric two-tailed *t*-test for statistical evaluation (McKnight & Najab, 2010), as normal distribution of fluorescence intensities was measured (Figure 2a, panels 1–3). Almost a half ($46.6 \pm 15.6\%$ on Day 6 and $49.7\% \pm 6.4\%$ on Day 8) of the cells was gated "bright" in the "feed" compared to almost non ($2.1 \pm 1.9\%$ for Day 6 and $1.9 \pm 0.4\%$ for Day 8) in the control (Figure 2a, panel 3). The "dim" gate showed the complementary inverted distribution (Figure 2a, panel 3). Thus, the observed cell volume gain in the "feed" is coupled with pronounced mitochondrial mass and activity boost.

The increase of mitochondrial activity observed in the "feed" on Day 6 and 8 of the fed-batch process is concomitant with its reduction in the "control" condition. As mitochondrial activity is correlated with protein synthesis and cell growth (Wahrheit et al., 2014), the observed decrease of mitochondrial fluorescence in "control" is most likely a manifestation of lower ATP synthesis rate by the cells entering a stationary phase. Such development of mitochondrial activity has been previously observed for hybridoma (Al-Rubeai et al., 1991) and CHO cells (Zagari et al., 2013) in the batch mode.

An existing study (Bi et al., 2004) reported a cell volume increase of CHO cells similar to that observed in our experiment following an overexpression of cyclin-dependent kinase inhibitor p21(CIP1). Increase of mitochondrial fluorescence accessed via MitoTracker FM Green dye correlating solely to mitochondrial mass was attributed to

the biogenesis of the new organelles and not to the activation of the existing ones. The authors also detected increased dehydrogenase activity in mitochondria. Another study suggests that osmolality elevation increases significantly the ATP-pool of the cell (Pfizenmaier et al., 2016; Pfizenmaier et al., 2015).

We suggest that our observation of increased mitochondrial fluorescence is most likely rooted in increased $\Delta\Psi_m$ polarization and/or size growth of existing mitochondria combined with the biogenesis of the new organelles. Although we recognize the limitation of the flow cytometry analysis to pinpoint the exact contributions of each of these effects, we believe that the upregulation of mitochondria plays a central role in CHO cellular response to osmotic stress.

3.2.2 | High-osmolality feed does not induce apoptosis in CHO DP-12 cells

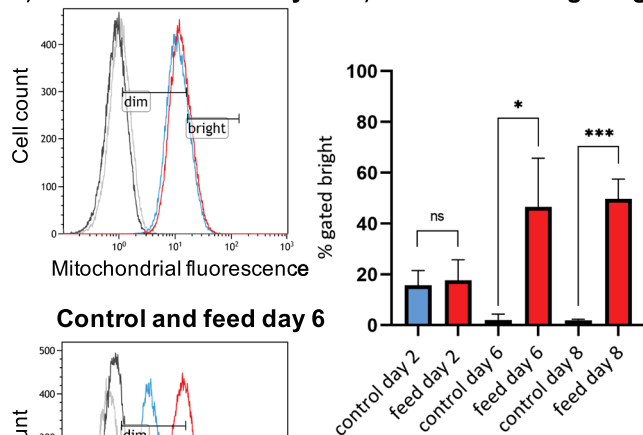
The available research data addressing apoptosis induction in osmotically stressed cells is rather ambivalent. Whether the cells die via apoptosis or necrosis upon exposure to hyper- or hypoosmotic pressure seems to depend on the cell type, severity of stress (Kim & Lee, 2002; Tao et al., 2002), and the agent used. Increased cellular apoptosis was observed in hybridoma (deZengotita et al., 2002), canine epithelial cells (Terada et al., 2001), and in antibody and EPO-producing rCHO cells (Han et al., 2010; Wang et al., 2012) where osmolality increase was induced by the addition of NaCl solution. On the other hand, kidney cells exhibited no apoptosis induction (Mak & Kültz, 2004) at 540 mOsm/kg, but did so upon even further (650–700 mOsm/kg) osmolality increase.

To assess if the high-osmolality feed induces apoptosis in the CHO cells in our set-up, we performed a Caspase 3/7 activation assay (Figure 2b). The activation of effector Caspases 3 and 7 is a rapid event marking the onset of the apoptotic death (Tyas et al., 2000). To exclude false-negative results, we verified the proper functionality of the assay in CHO DP-12 cells by inducing apoptosis with staurosporine ($0.5 \mu\text{M}$, 5 h incubation) and applying the same staining and measurement protocol. We were able to detect about 30% of bright green cells (data not shown) confirming

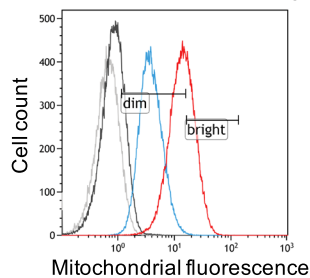
FIGURE 1 Fed-batch cultivation of Chinese hamster ovary (CHO) DP-12 cells, based on three biological replicates per condition. (control vs. feed) (a) Viable cell density VCD, [$\times 10^5$ cells/ml], and viability [%] for control and feed conditions. Black vertical lines indicate the addition of 6 ml supplemented feed to "feed" shakers and growth medium to "control" shakers; (b) osmolality [mOsm/kg] and mean cell diameter [μm] during the fed-batch cultivation; (c) The cell size distribution measured by Cedex AS 20 during the fed-batch cultivation of the DP-12 cells, attributed to three gates 12.5–18 μm , 18–25 μm , > 25 μm . (d) Average antibody concentration [mg/ml] and cell-specific productivity qP [pg/cell \times day] during the fed-batch cultivation of CHO DP-12 cells, based on three biological replicates per condition. The antibody concentrations after 24 and 48 h are below the limit of detection and thus could not be estimated. (e) The cell cycle distribution analysis on Days 2, 4, 5, and 7 for the fed-batch cultivation of CHO DP-12 cells. The upper row shows the control condition and the lower row the feed condition. For each condition and time point, the propidium iodide (PI) stain intensity (FL2-H) is shown as a function of a linear count histogram. Cell debris was gated out based on FSC-A versus SSC-A dot plot, cell aggregates based on FSC-H versus FSC-A diagonal plot. Three biological replicates were measured for each condition and time point. FL-2H indicates the amount of DNA in the cell. The events measured at intensity over 2000 are most likely to be caused by unresolved cell doublets or natural polyploidy of the CHO cells [Color figure can be viewed at wileyonlinelibrary.com]

(a) Mitochondrial fluorescence

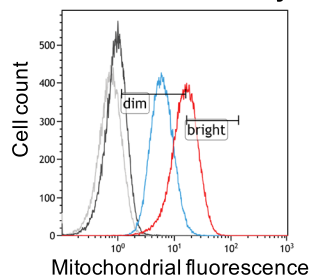
1) Control and feed day 2 2) Cells in the "bright" gate



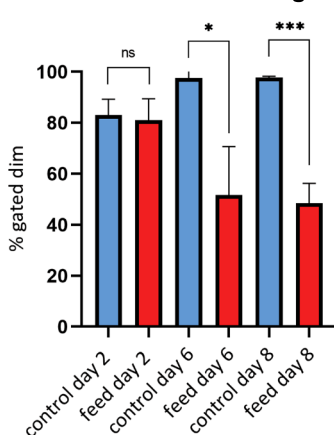
Control and feed day 6



Control and feed day 8



3) Cells in the "dim" gate



(b) Caspase activity

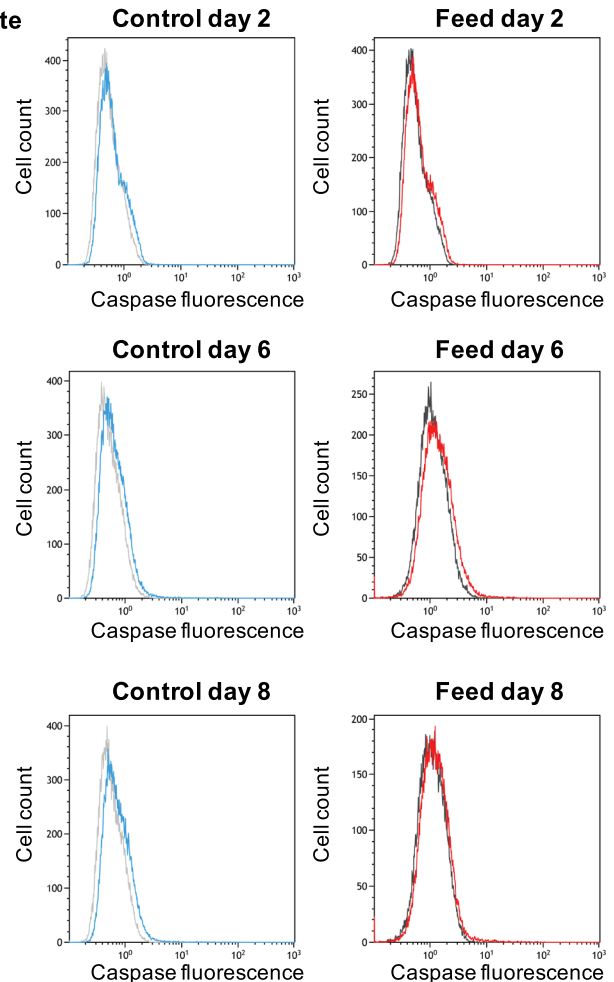


FIGURE 2 (a) The flow cytometry analysis of mitochondria activity on Days 2, 6, and 8 for the fed-batch cultivation of CHO DP-12 cells. (1) Difference in mitochondrial fluorescence measured by flow cytometry on Days 2, 6, and 8. The x-axis—log-scale FL6-A fluorescence intensity (corresponding to mitochondrial fluorescence); the y-axis—the linear events count. Unstained (gray) and MitoTracker®CMXRos-stained (blue for control and red for feed) cell populations for one biological replicate are shown as an example for each time point. Cell debris (based on FSC-A vs. SSC-A dot plot), cell aggregates (based on FSC-H vs. FSC-A diagonal plot), and dead cells (based on DAPI nuclear stain, measured in FL1-A channel) were gated out. Gates “dim” and “bright” were applied uniformly to all measured samples. (2) and (3) Graphical representation of mitochondrial fluorescence data showing a percentage of the cells in the “bright” and “dim” gate of FL6-A ($n = 3$). Statistical evaluation was performed by an unpaired parametric two-tailed *t*-test ($*p$ -value < 0.05 ; $***p$ -value < 0.0005); (b) The flow cytometry analysis of Caspase 3/7 activation on Days 2, 6, and 8 for the fed-batch cultivation of CHO DP-12 cells. The graphs are plotted in log-scale FL2-A (Caspase fluorescence, x-axis) against the linear events count (y-axis). Unstained (grey) and Caspase 3/7 Green detection Reagent-stained (blue for control and red for feed) cell populations for one biological replicate is shown as an example for each time point. Cell debris was gated out based on FSC-A versus SSC-A dot plot, cell aggregates based on FSC-H versus FSC-A diagonal plot and dead cells based on DAPI nuclear stain, measured in FL1-A channel. CHO, Chinese hamster ovary; DAPI, 4',6-diamidino-2-phenylindole [Color figure can be viewed at wileyonlinelibrary.com]

that observing no Caspase 3/7 activation is not caused by invalid assay performance.

Our experimental results show indeed no signs of early apoptosis during the fed-batch cultivation of CHO DP-12 cells throughout all three sampling points (Days 2, 6, and 8) in both control and feed conditions ($n = 3$ for each condition). No shift in fluorescence was observed in the FL-1 channel at 514 nm between stained and unstained cell populations (see Figure 2b), affirming no programmed cell death induction either in osmotically stressed “feed” or normally

cultivated “control” cells. This result was reproduced throughout at least three independent cultivations.

Apoptosis is a very multifarious and complex process. Its regulation, signaling, and antiapoptotic engineering have been extensively studied in CHO cells and are regularly reviewed (Henry et al., 2020; Krampe & Al-Rubeai, 2010) in literature. It seems that apoptosis is not an imminent part of osmolality-induced stress response in general but is rather activated if, for example, vital nutrients are concurrently depleted in the culture (Han et al., 2011;

Hwang & Lee, 2008). As we used a complete supplemented feed solution specifically designed for CHO cells, we presume that no substrate limitations occurred in the feed condition during the fed-batch process, thus explaining why the CHO DP-12 cells did not induce apoptosis in our experiment.

3.3 | Single-cell observation via confocal microscopy and ICC

We next validated our flow cytometry analysis by analyzing the mitochondria amount and activity in CHO DP-12 cells exposed to high osmolality feed conditions using ICC. The cells were sampled on Days 2, 6, and 8, stained with 200 nM MitoTracker® Red CMXRos (Cell Signalling Technology Inc.) and imaged using confocal laser scanning microscopy (Figure 3a,b). The first sample (Day 2) served as a reference point before feed or supplemented medium addition. As expected, no differences in the amount of mitochondrial fluorescence in

CHO cells were observed (2 days of culture; Figure 3a). On Day 8 (Figure 3b), only a slight tendency towards mitochondrial fluorescence increase can be observed in “feed” cells with respect to “control” (Figure 3b). One should keep in mind that cells lose their mitochondrial membrane potential upon fixation and permeabilization, thus the dye can be used primarily for mitochondrial localization and rough abundance determination. Besides, we have performed antibody-based staining of S6 ribosomal protein (54D2) to detect its total endogenous level in cells. Ribosomal protein S6 is a part of the ribosomal S40 subunit. Its phosphorylation has been reported to be related to cell size regulation and cell cycle progression (Ruvinsky et al., 2005; Ruvinsky & Meyuhas, 2006). Although we did measure a slight S6 abundance increase via LFQ tandem mass spectrometry (please refer to electronic supplementary material of the article: Hyperosmolality in CHO Culture: Effects on Proteome) (\log_2 fold change F vs. C D6 +0.11, D8 +0.01), this change is scarcely detectable by eye indicating that feed-based increase in cell size might be based on an S6-independent mechanism. The population-level cell size increase measured via

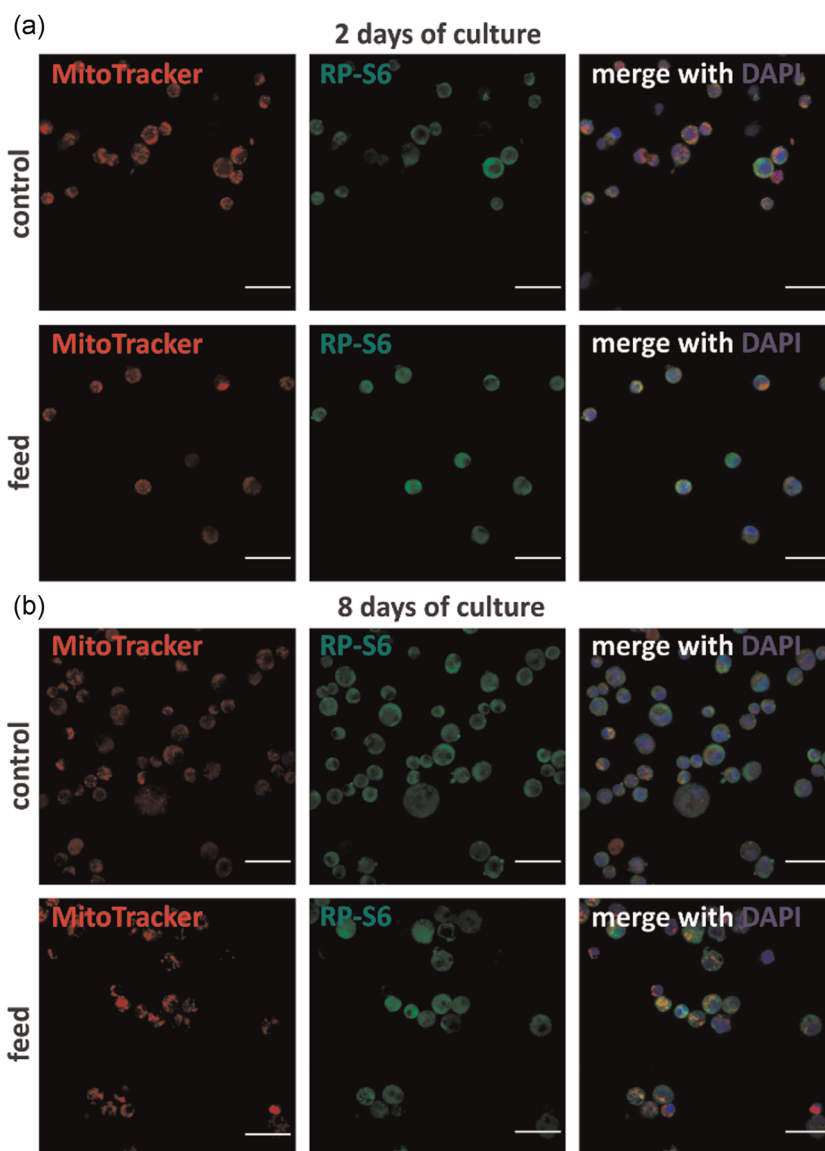


FIGURE 3 Immunocytochemical analysis of mitochondrial and ribosomal staining on Days 2 and 8 under fed-batch conditions of CHO-DP12 cells exposed to high osmolality (“feed”) or without osmotic changes (“control”). (a) and (b) Cells on Days 2 and 8 of the fed-batch cultivation centrifuged down on μ -slide 8 well chamber slides and stained with MitoTracker® Red CMXRos, the primary antibody against 40S ribosomal protein S6 and DAPI. The primary antibody was visualized with secondary Antibody Alexa Fluor 488. CHO, Chinese hamster ovary; DAPI, 4',6-diamidino-2-phenylindole [Color figure can be viewed at wileyonlinelibrary.com]

Cedex AS20 was not observable via ICC because mounting the cells on the slide surface inhomogeneously altered their initial spherical form.

3.3.1 | CHO DP-12 cells treated with high osmolality feed reveal significantly increased amounts of nuclei per cell

To evaluate the impact of high osmolality feed on cell nucleus morphology, CHO cells treated with feed for 4 and 6 days (Days 6 and 8 of the fed-batch) were stained with DAPI and phalloidin rhodamine. On reference Day 2 (48 h after seeding) no significant changes in the number or shape of nuclei of CHO cells were observable (Figures 4a and 4c). The cells displayed mostly uniform round-shaped single nuclei both in control and feed populations. On Days 6 and 8 the CHO cells in the feed condition showed a highly significant increase in the number of nuclei or the presence of

micronuclei (Figure 4b, arrows) compared to the control condition (Figure 4b, arrowheads).

Micronuclei are formed during cell division when acentric chromosome fragments or whole chromosomes that were not incorporated into the main nuclei during cell division are enclosed by a nuclear membrane (Fenech & Morley, 1985). Micronuclei were reported to be a biomarker for multipolar anaphase, genotoxic effects, and chromosome aberration (Norppa, 2003; Pastor et al., 2009). In accordance with our findings, changes in osmolality were already shown to cause the formation of micronuclei (Fenech et al., 2010; Henderson et al., 2000; Meintières & Marzin, 2004), but not for the CHO cells. In particular, Meintières and Marzin (2004) observed the exposure of mouse lymphocyte CTLL-2 cells to high osmolality by NaCl to result in the formation of micronuclei. To the best of our knowledge, the formation of micronuclei in CHO cells exposed to osmolality increase has not been observed previously. Meintières and Marzin (2004) further demonstrated micronuclei formation to be accompanied by increased apoptosis of CTLL-2 cells exposed to

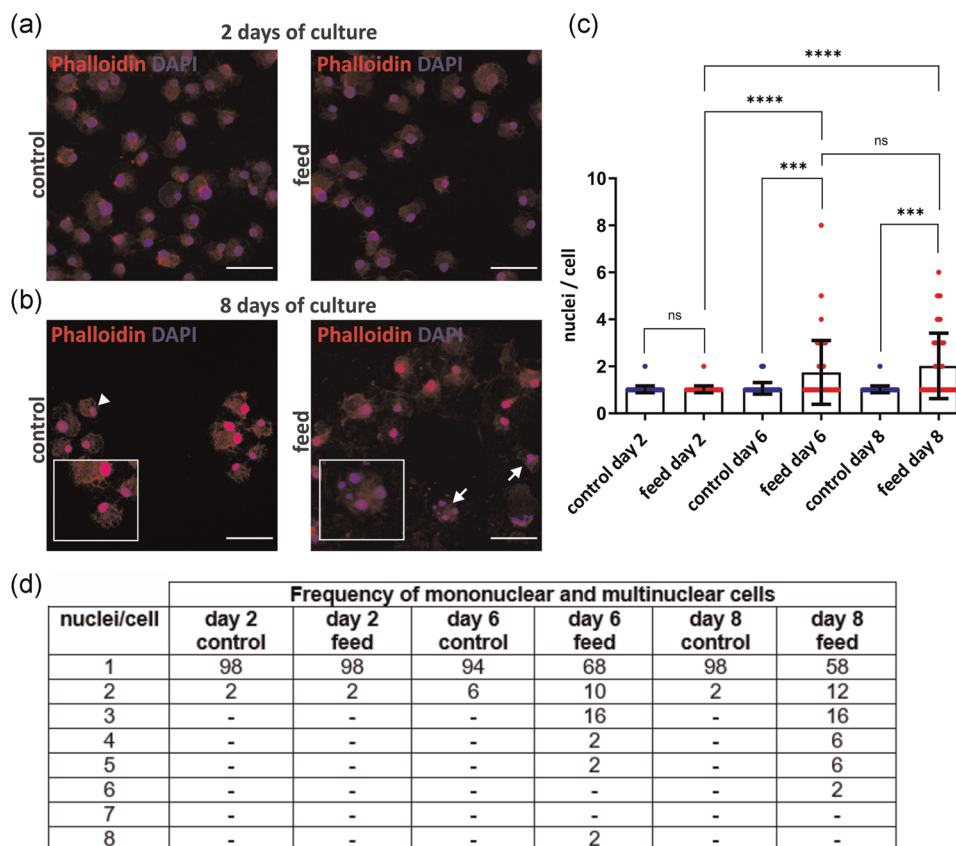


FIGURE 4 Immunocytochemical analysis of cytoskeleton and nuclear morphology across three cultivation time points for fed-batch cultivation of CHO-DP12 cells to high osmolality feed (“feed”) or without osmotic change (“control”). (a) and (b) 2 and 8 days of cultivation centrifuged down on μ -slide 8 well chamber slides and stained with phalloidin rhodamine and DAPI. (c) Quantification and comparison of micronuclei formation on Day 2, 6, and 8 between feed and control conditions; statistical significance by an unpaired parametric two-tailed *t*-test with the statistically significant threshold of **p* value < 0.05; ****p*-value < 0.0005. (d) Frequency of normal versus multinucleated cells. For each condition, the nuclei amount of 50 cells were counted and the relative frequency of the normal versus multinucleated cells were calculated. Day 2 control: 98% normal 2% multinucleated; Day 2 feed: 98% normal 2% multinucleated; Day 6 control: 94% normal 6% multinucleated; Day 6 feed: 68% normal, 32% multinucleated; Day 8 control: 98% normal 2% multinucleated; Day 8 feed: 58% normal, 42% multinucleated. CHO, Chinese hamster ovary; DAPI, 4',6-diamidino-2-phenylindole [Color figure can be viewed at wileyonlinelibrary.com]

NaCl. On the contrary, our present findings revealed an increased amount of micronuclei in CHO cells after high osmolality feed without induction of apoptosis (Figure 2b).

We suppose that nuclear shape alterations in CHO cells are probably a direct result of osmotically induced stress. A recent finding reveals that exposure to elevated ROS concentrations induces nuclear shape alterations including fragmentation and folding due to aberrations in the reassembly of the nuclear envelope in cancer cells (Ahn et al., 2019). The authors discovered that the cells are most vulnerable during mitosis, so it is unclear if the structures we observed on Days 6 and 8 in the “feed” condition are artifacts of uncompleted mitotic division disrupted by osmolality increase on Day 3/4 or if these have evolved during the fed-batch gradually with time.

4 | CONCLUSIONS

The increased osmolality response of mammalian cells differs principally from that of bacteria. It was shown that *Escherichia coli* cells lose water and decrease in the cell size proportional to extrinsic osmolality increase (Dai & Zhu, 2018). The mammalian cells on the contrary show the expected cell volume decrease due to cytoplasmic fluids loss only in the first hours of osmotic shock. After this, the cells cease to proliferate but continue to produce biomass, achieving significantly larger cell diameter, and cell volume.

Although effects of osmolality change in respect to productivity and growth of CHO cells have been a topic of several studies in the past few years (Kiehl et al., 2011; Pan et al., 2017; Shen et al., 2010; Takagi et al., 2000), we used a combined multilevel approach for the first time. Our results suggest that osmolality increase causes substantial adaptation effects, involving mitochondria activation, proliferation arrest, cell-size increase, and formation of multiple nuclei in some cells. We also showed that hyperosmolality does not necessarily trigger an increase in cell-specific productivity (qP). Numerous data suggest that the cell generates a surplus of energy under osmotic pressure. This was documented based on increased oxygen and glucose uptake rates (Lin et al., 1999; Pfizenmaier et al., 2015; Takagi et al., 2000), ATP-pool enhancement (Pfizenmaier et al., 2016), and increase in mitochondrial membrane potential, as shown by our experiments. These findings point to a question of how does the cell channel the excess energy that should be addressed in further research. To tackle this issue, we conducted an LFQ proteome analysis. Preliminary data supports substantial increase of mitochondrial function on protein level and gives hints to the ways the gained energy is utilized.

Although the topic of hyperosmolality effects has been addressed by numerous research projects, hardly any of them analyzed systematically the specific influences of the added agents. As the data on the topic continues to accumulate, it will be necessary to address this issue in the upcoming projects via multiple comparison cultivations using different substances to control osmolality.

ACKNOWLEDGMENTS

The authors would like to thank Nele v. Vegesack for her assistance with preliminary experiments and live stains sample preparation. This study was funded by Bielefeld University. Nadiya Romanova is supported by a Grant for women in the orientation phase initiated by the Equal Opportunities Commission of the Faculty of Technology, Bielefeld University.

CONFLICT OF INTERESTS

The authors declare that there are no conflict of interests.

AUTHOR CONTRIBUTIONS

N. Romanova designed the experiments, carried out cell cultivation, sample preparation, analyzed and interpreted the data, and wrote the manuscript. T. Niemann contributed to experiment design, performed the flow cytometry measurements (live stains), immunocytochemical sample preparation and analysis, evaluated the data, and wrote the manuscript. J. FW Greiner contributed to data analysis and interpretation, flow cytometry troubleshooting, and preparation of the manuscript. B. Kaltschmidt and C. Kaltschmidt contributed to experiment design and supervised the project. T. Noll conceived an initial project idea, acquired funding and supervised the project. All authors read and edited the manuscript.

DATA AVAILABILITY STATEMENT

Data available on request from the authors.

ORCID

Johannes F. W. Greiner  <http://orcid.org/0000-0002-0524-662X>

Thomas Noll  <http://orcid.org/0000-0003-0748-3423>

REFERENCES

- Ademowo, O. S., Dias, H. K. I., Burton, D. G. A., & Griffiths, H. R. (2017). Lipid (per) oxidation in mitochondria: An emerging target in the ageing process? *Biogerontology*, 18(6), 859–879. <https://pubmed.ncbi.nlm.nih.gov/28540446>
- Ahn, J.-H., Cho, M.-G., Sohn, S., & Lee, J.-H. (2019). Inhibition of PP2A activity by H₂O₂ during mitosis disrupts nuclear envelope reassembly and alters nuclear shape. *Experimental & Molecular Medicine*, 51(6), 1–18. <https://doi.org/10.1038/s12276-019-0260-0>
- Alexander, M. R., Tyers, M., Perret, M., Craig, B. M., Fang, K. S., & Gustin, M. C. (2001). Regulation of cell cycle progression by SWE1P and HOG1P following hypertonic stress. *Molecular Biology of the Cell*, 12(1), 53–62. <https://doi.org/10.1091/mbc.12.1.53>
- Al-Rubeai, M., Chalder, S., Bird, R., & Emery, A. N. (1991). Cell cycle, cell size and mitochondrial activity of hybridoma cells during batch cultivation. *Cytotechnology*, 7(3), 179–186. <https://doi.org/10.1007/BF00365929>
- Bi, J.-X., Shuttleworth, J., & Al-Rubeai, M. (2004). Uncoupling of cell growth and proliferation results in enhancement of productivity in p21CIP1-arrested CHO cells. *Biotechnology and Bioengineering*, 85(7), 741–749.
- Bibila, T. A., & Robinson, D. K. (1995). In pursuit of the optimal fed-batch process for monoclonal antibody production. *Biotechnology Progress*, 11(1), 1–13.
- Cadart, C., Monnier, S., Grilli, J., Sáez, P. J., Srivastava, N., Attia, R., Terriac, E., Baum, B., Cosentino-Lagomarsino, M., & Piel, M. (2018).

- Size control in mammalian cells involves modulation of both growth rate and cell cycle duration. *Nature Communications*, 9(1), 3275. <https://doi.org/10.1038/s41467-018-05393-0>
- Chan, D. C. (2006). Mitochondria: Dynamic organelles in disease, aging, and development. *Cell*, 125(7), 1241–1252.
- Cottet-Rousselle, C., Ronot, X., Leverve, X., & Mayol, J.-F. (2011). Cytometric assessment of mitochondria using fluorescent probes. *Cytometry, Part A*, 79A(6), 405–425. <https://doi.org/10.1002/cyto.a.21061>
- Dai, X., & Zhu, M. (2018). High osmolarity modulates bacterial cell size through reducing initiation volume in *Escherichia coli*. *mSphere*, 3(5).
- Demidenko, Z. N., & Blagosklonny, M. V. (2008). Growth stimulation leads to cellular senescence when the cell cycle is blocked. *Cell Cycle*, 7(21), 3355–3361.
- deZengotita, V. M., Schmelzer, A. E., & Miller, W. M. (2002). Characterization of hybridoma cell responses to elevated pCO₂ and osmolality: Intracellular pH, cell size, apoptosis, and metabolism. *Biotechnology and Bioengineering*, 77(4), 369–380. <https://doi.org/10.1002/bit.10176>
- Fenech, M., Kirsch-Volders, M., Natarajan, A. T., Surrallés, J., Crott, J. W., Parry, J., Norppa, H., Eastmond, D. A., Tucker, J. D., & Thomas, P. (2010). Molecular mechanisms of micronucleus, nucleoplasmic bridge and nuclear bud formation in mammalian and human cells. *Mutagenesis*, 26(1), 125–132.
- Fenech, M., & Morley, A. A. (1985). Measurement of micronuclei in lymphocytes. *Mutation Research/Environmental Mutagenesis and Related Subjects*, 147(1-2), 29–36.
- Fischer, S., Handrick, R., & Otte, K. (2015). The art of CHO cell engineering: A comprehensive retrospect and future perspectives. *Biotechnology Advances*, 33(8), 1878–1896.
- Gilson, P. R., Yu, X.-C., Hereld, D., Barth, C., Savage, A., Kiefel, B. R., Lay, S., Fisher, P. R., Margolin, W., & Beech, P. L. (2003). Two dictyostelium orthologs of the prokaryotic cell division protein FTSZ localize to mitochondria and are required for the maintenance of normal mitochondrial morphology. *Eukaryotic Cell*, 2(6), 1315–1326. <https://pubmed.ncbi.nlm.nih.gov/14665465>
- Han, Y. K., Ha, T. K., Lee, S. J., Lee, J. S., & Lee, G. M. (2011). Autophagy and apoptosis of recombinant Chinese hamster ovary cells during fed-batch culture: Effect of nutrient supplementation. *Biotechnology and Bioengineering*, 108(9), 2182–2192.
- Han, Y. K., Kim, Y.-G., Kim, J. Y., & Lee, G. M. (2010). Hyperosmotic stress induces autophagy and apoptosis in recombinant Chinese hamster ovary cell culture. *Biotechnology and Bioengineering*, 105(6), 1187–1192. <https://doi.org/10.1002/bit.22643>
- Hayashi, M., Norppa, H., Sofuni, T., & Ishidate, M. (1992). Mouse bone marrow micronucleus test using flow cytometry. *Mutagenesis*, 7(4), 251–256.
- Henderson, L., Albertini, S., & Aardema, M. (2000). Thresholds in genotoxicity responses. *Mutation Research/Genetic Toxicology and Environmental Mutagenesis*, 464(1), 123–128.
- Henry, M. N., MacDonald, M. A., Orellana, C. A., Gray, P. P., Gillard, M., Baker, K., Nielsen, L. K., Marcellin, E., Mahler, S., & Martinez, V. S. (2020). Attenuating apoptosis in Chinese hamster ovary cells for improved biopharmaceutical production. *Biotechnology and Bioengineering*, 117(4), 1187–1203. <https://doi.org/10.1002/bit.27269>
- Hwang, S. O., & Lee, G. M. (2008). Nutrient deprivation induces autophagy as well as apoptosis in Chinese hamster ovary cell culture. *Biotechnology and Bioengineering*, 99(3), 678–685. <https://doi.org/10.1002/bit.21589>
- Ryu, J. S., & Lee, G. M. (1999). Application of hypoosmolar medium to fed-batch culture of hybridoma cells for improvement of culture longevity. *Biotechnology and Bioengineering*, 62.1, 120–123.
- Kiehl, T. R., Shen, D., Khattak, S. F., Jian Li, Z., & Sharfstein, S. T. (2011). Observations of cell size dynamics under osmotic stress. *Cytometry, Part A*, 79A(7), 560–569. <https://doi.org/10.1002/cyto.a.21076>
- Kim, J. Y., Kim, Y.-G., & Lee, G. M. (2011). CHO cells in biotechnology for production of recombinant proteins: Current state and further potential. *Applied Microbiology and Biotechnology*, 93(3), 917–930.
- Kim, N. S., & Lee, G. M. (2002). Response of recombinant Chinese hamster ovary cells to hyperosmotic pressure: effect of bcl-2 overexpression. *Journal of Biotechnology*, 95(3), 237–248.
- Krampe, B., & Al-Rubeai, M. (2010). Cell death in mammalian cell culture: Molecular mechanisms and cell line engineering strategies. *Cytotechnology*, 62(3), 175–188. <https://pubmed.ncbi.nlm.nih.gov/20502964>
- Li, Y., Almossalha, L. M., Chandler, J. E., Zhou, X., Stypula-Cyrus, Y. E., Hujsak, K. A., Roth, E. W., Bleher, R., Subramanian, H., Szeleifer, I., Dravid, V. P., & Backman, V. (2017). The effects of chemical fixation on the cellular nanostructure. *Experimental Cell Research*, 358(2), 253–259. <http://www.sciencedirect.com/science/article/pii/S001448271730352X>
- Lin, P., Yao, Y., Hofmeister, R., Tsien, R. Y., & Farquhar, M. G. (1999). Overexpression of calnexin (nucleobindin) increases agonist and thapsigargin releasable Ca²⁺ storage in the Golgi. *The Journal of Cell Biology*, 145(2), 279–289. <https://pubmed.ncbi.nlm.nih.gov/10209024>
- Macho, A., Decaudin, D., Castedo, M., Hirsch, T., Susin, S. A., Zamzami, N., & Kroemer, G. (1996). Chloromethyl-X-rosamine is an aldehyde-fixable potential-sensitive fluorochrome for the detection of early apoptosis. *Cytometry*, 25(4), 333–340.
- Mak, S. K., & Kültz, D. (2004). Gadd45 proteins induce g2/m arrest and modulate apoptosis in kidney cells exposed to hyperosmotic stress. *Journal of Biological Chemistry*, 279(37), 39075–39084.
- McKnight, P. E., & Najab, J. (2010). 'Mann-Whitney U test'. <https://online-library.wiley.com/doi/abs/10.1002/9780470479216.corpsy0524>
- Meintières, S., & Marzin, D. (2004). Apoptosis may contribute to false-positive results in the in vitro micronucleus test performed in extreme osmolality, ionic strength and pH conditions. *Mutation Research/Genetic Toxicology and Environmental Mutagenesis*, 560(2), 101–118.
- Nasseri, S. S., Ghaffari, N., Braasch, K., Jardon, M. A., Butler, M., Kennard, M., Gopaluni, B., & Piret, J. M. (2014). Increased cho cell fed-batch monoclonal antibody production using the autophagy inhibitor 3-MA or gradually increasing osmolality. *Biochemical Engineering Journal*, 91, 37–45. <http://www.sciencedirect.com/science/article/pii/S1369703X1400206X>
- Neurohr, G. E., Terry, R. L., Lengefeld, J., Bonney, M., Brittingham, G. P., Moretto, F., Miettinen, T. P., Vaites, L. P., Soares, L. M., Paulo, J. A., Harper, J. W., Buratowski, S., Manalis, S., van Werven, F. J., Holt, L. J., & Amon, A. (2019). Excessive cell growth causes cytoplasm dilution and contributes to senescence. *Cell*, 176(5), 1083–1097. <http://www.sciencedirect.com/science/article/pii/S0092867419300510>
- Norppa, H. (2003). What do human micronuclei contain? *Mutagenesis*, 18(3), 221–233.
- Pan, X., Alsayyari, A. A., Dalm, C., Hageman, J. A., Wijffels, R., & Martens, D. E. (2019). Transcriptome analysis of cho cell size increase during a fed-batch process. *Biotechnology Journal*, 14(3), 1800156. <https://doi.org/10.1002/biot.201800156>
- Pan, X., Dalm, C., Wijffels, R., & Martens, D. E. (2017). Metabolic characterization of a cho cell size increase phase in fed-batch cultures. *Applied Microbiology and Biotechnology*, 101(22), 8101–8113. <https://www.ncbi.nlm.nih.gov/pubmed/28951949>
- Pastor, N., Kaplan, C., Domnguez, I., Mateos, S., & Cortés, F. (2009). Cytotoxicity and mitotic alterations induced by non-genotoxic lithium salts in CHO cells in vitro. *Toxicology In Vitro*, 23(3), 432–438.

- Pendergrass, W., Wolf, N., & Poot, M. (2004). Efficacy of mitotracker green and cmxrosamine to measure changes in mitochondrial membrane potentials in living cells and tissues. *Cytometry: Part A*, 61(2), 162–169.
- Pfizenmaier, J., Junghans, L., Teleki, A., & Takors, R. (2016). Hyperosmotic stimulus study discloses benefits in atp supply and reveals miRNA/mRNA targets to improve recombinant protein production of cho cells. *Biotechnology Journal*, 11(8), 1037–1047.
- Pfizenmaier, J., Matuszczyk, J.-C., & Takors, R. (2015). Changes in intracellular ATP-content of CHO cells as response to hyperosmolality. *Biotechnology Progress*, 31(5), 1212–1216.
- Poot, M., Zhang, Y. Z., Krämer, J. A., Wells, K. S., Jones, L. J., Hanzel, D. K., Lugade, A. G., Singer, V. L., & Haugland, R. P. (1996). Analysis of mitochondrial morphology and function with novel fixable fluorescent stains. *Journal of Histochemistry and Cytochemistry*, 44(12), 1363–1372.
- Pratt, P. L., Bryce, J. H., & Stewart, G. G. (2003). The effects of osmotic pressure and ethanol on yeast viability and morphology. *Journal of the Institute of Brewing*, 109(3), 218–228.
- Puleston, D. (2015). Detection of mitochondrial mass, damage, and reactive oxygen species by flow cytometry. *Cold Spring Harbor Protocols*, 2015(9):pdb.prot086298.
- Qin, J., Wu, X., Xia, Z., Huang, Z., Zhang, Y., Wang, Y., Fu, Q., & Zheng, C. (2019). The effect of hyperosmolality application time on production, quality, and biopotency of monoclonal antibodies produced in CHO cell fed-batch and perfusion cultures. *Applied Microbiology and Biotechnology*, 103(3), 1217–1229.
- Schliess, F., Reinehr, R., & Häussinger, D. (2007). Osmosensing and signaling in the regulation of mammalian cell function. *FEBS Journal*, 274(22), 5799–5803.
- Shen, D., Kiehl, T. R., Khattak, S. F., Li, Z. J., He, A., Kayne, P. S., Patel, V., Neuhaus, I. M., & Sharfstein, S. T. (2010). Transcriptomic responses to sodium chloride-induced osmotic stress: A study of industrial fed-batch CHO cell cultures. *Biotechnology Progress*, 26(4), 1104–1105.
- Takagi, M., Hayashi, H., & Yoshida, T. (2000). The effect of osmolarity on metabolism and morphology in adhesion and suspension Chinese hamster ovary cells producing tissue plasminogen activator. *Cytotechnology*, 32(3), 171–179.
- Tao, G.-Z., Rott, L. S., Lowe, A. W., & Omary, M. B. (2002). Hyposmotic stress induces cell growth arrest via proteasome activation and cyclin/cyclin-dependent kinase degradation. *Journal of Biological Chemistry*, 277(22), 19295–19303.
- Tarnowski, B. I., Spinale, F. G., & Nicholson, J. H. (1991). DAPI as a useful stain for nuclear quantitation. *Biotechnic & Histochemistry*, 66(6), 296–302.
- Terada, Y., Inoshita, S., Hanada, S., Shimamura, H., Kuwahara, M., Ogawa, W., Kasuga, M., Sasaki, S., & Marumo, F. (2001). Hyperosmolality activates akt and regulates apoptosis in renal tubular cells. *Kidney International*, 60(2), 553–567. <http://www.sciencedirect.com/science/article/pii/S0085253815479001>
- Tyas, L., Brophy, V. A., Pope, A., Rivett, A. J., & Tavaré, J. M. (2000). Rapid caspase-3 activation during apoptosis revealed using fluorescence-resonance energy transfer. *EMBO Reports*, 1(3), 266–270. <https://pubmed.ncbi.nlm.nih.gov/11256610>
- Wahrheit, J., Niklas, J., & Heinzle, E. (2014). Metabolic control at the cytosol-mitochondria interface in different growth phases of cho cells. *Metabolic Engineering*, 23, 9–21. <http://www.sciencedirect.com/science/article/pii/S109671761400007X>
- Walsh, G. (2018). Biopharmaceutical benchmarks 2018. *Nature Biotechnology*, 36(12), 1136–1145.
- Wang, Z., Ma, X., Zhao, L., Fan, L., & Tan, W.-S. (2012). Expression of anti-apoptotic 30KC6 gene inhibiting hyperosmotic pressure-induced apoptosis in antibody-producing Chinese hamster ovary cells. *Process Biochemistry*, 47(5), 735–741. <http://www.sciencedirect.com/science/article/pii/S1359511312000657>
- Zagari, F., Jordan, M., Stettler, M., Broly, H., & Wurm, F. M. (2013). Lactate metabolism shift in CHO cell culture: The role of mitochondrial oxidative activity. *New Biotechnology*, 30(2), 238–245.
- Ruvinsky Igor, Meyuhas Oded (2006). Ribosomal protein S6 phosphorylation: from protein synthesis to cell size. *Trends in Biochemical Sciences*, 31, (6), 342–348. <http://dx.doi.org/10.1016/j.tibs.2006.04.003>.
- Ruvinsky I. (2005). Ribosomal protein S6 phosphorylation is a determinant of cell size and glucose homeostasis. *Genes & Development*, 19, (18), 2199–2211. <http://dx.doi.org/10.1101/gad.351605>

How to cite this article: Romanova, N., Niemann, T., Greiner, J. F. W., Kaltschmidt, B., Kaltschmidt, C., & Noll, T. (2021). Hyperosmolality in CHO culture: Effects on cellular behavior and morphology. *Biotechnology and Bioengineering*. 118, 2348–2359. <https://doi.org/10.1002/bit.27747>